# Modal Behavior of the $\mu$1 $Na^+$ Channel and Effects of Coexpression of the $\beta_1$-Subunit

Steven Y. Chang,* Jonathan Satin,‡ and Harry A. Fozzard*
*Department of Pharmacological and Physiological Sciences, The University of Chicago, Chicago, Illinois, and ‡Department of Physiology, The University of Kentucky, Lexington, Kentucky, USA

ABSTRACT The adult rat skeletal muscle $Na^+$ channel $\alpha$-subunit ($\mu$1) appears to gate modally with two kinetic schemes when the channel is expressed in *Xenopus* oocytes. In the fast mode $\mu$1 single channels open only once or twice per depolarizing pulse, but in the slow mode the channels demonstrate bursting behavior. Slow-mode gating was favored by hyperpolarized holding potentials and slow depolarizing rates, whereas fast-mode gating was favored by depolarized holding potentials and rapid depolarizations. Single-channel studies showed that coexpression of $\beta_1$ reduces slow-mode gating, so that channels gate almost exclusively in the fast mode. Analysis of open-time histograms showed that $\mu$1 and $\mu$1 + $\beta_1$ both have two open-time populations with the same mean open times (MOTs). The difference lies in the relative sizes of the long and short MOT components. When $\beta_1$ was coexpressed with $\mu$1 in oocytes, the long MOT fraction was greatly reduced. It appears that although $\mu$1 and $\mu$1 + $\beta_1$ share the same two open states, the $\beta_1$-subunit favors the mode with the shorter open state. Examination of first latencies showed that it is likely that the rate of activation is increased upon coexpression with $\beta_1$. Experiments also showed that the rate of activation for the fast mode of $\mu$1 is identical to that for $\mu$1 + $\beta_1$ and is thus more rapid than the rate of activation for the slow mode. It can be concluded that $\beta_1$ restores native-like kinetics in $\mu$1 by favoring the fast-gating mode.

## INTRODUCTION

Expression in *Xenopus laevis* oocytes of rat brain IIa (rBr2a) or of adult rat skeletal muscle ($\mu$1) results in functional channels with abnormally slow $Na^+$ current ($I_{Na}$) decay kinetics (Goldin et al., 1986; Trimmer et al., 1989; Satin et al., 1992). Coexpression of the rat brain $\beta_1$-subunit ($\beta_1$) with rBr2a or $\mu$1 in oocytes accelerates $I_{Na}$ decay kinetics toward normal (Isom et al., 1992; Cannon et al., 1993; Yang et al., 1993; Wallner et al., 1993; Patton et al., 1994). The underlying mechanism by which $\beta_1$ alters rBr2a and $\mu$1 $\alpha$-subunit kinetics has not been resolved; it could create a new kinetic pattern (Schreibmayer et al., 1994) or it could reduce the prevalence of a normally occurring slow inactivation mode. Zhou et al. (1991) and Moorman et al. (1990) have suggested that the current kinetics of $\mu$1 and rat brain III (rBr3) $\alpha$-subunits expressed in *Xenopus* oocytes without $\beta_1$ are modal. Single-channel studies by Moorman et al. (1990) showed that the slow macroscopic $I_{Na}$ decay of rBr3 resulted from an excessive amount of bursting activity. Zhou et al. (1991) found that coexpression of $\mu$1 with a low-molecular-weight fraction of brain mRNA, presumably containing a message for the $\beta_1$-subunit, diminished bursting activity and replaced it with single, short openings. In their experiments, ensemble averages of $\mu$1 coexpressed with the low-molecular-weight mRNA demonstrated rapid $I_{Na}$ decay (Zhou et al., 1991).

Identification of modal kinetics requires that more than one kinetic scheme be present in a single data set, and that the various kinetic schemes be nonrandomly distributed. A third criterion suggested by Nilius (1988) that the different kinetic schemes should be inducible facilitates their study. Mode switching has been described for several channel types, including glutamate channels (Patlak et al., 1979) and acetylcholine-gated channels (Naranjo and Brehm, 1993), various voltage-gated channels (Hess et al., 1984; Patlak and Ortiz, 1985, 1986; Nilius, 1988; Plummer and Hess, 1991; Delcour et al., 1993; Delcour and Tsien, 1993; Alzheimer et al., 1993; Böhle and Benndorf, 1995), and $Ca^{2+}$-activated $K^+$ channels (Moczydlowski and Latorre, 1983; McManus and Magelby, 1988). If Zhou et al. (1991) and Moorman et al. (1990) are correct about the modal behavior of Na channel $\alpha$-subunits, then it is plausible that the $\beta_1$-subunit might exert its effects simply by favoring the fast gating mode. Using oocyte-attached patches and inside-out patch recordings of $Na^+$ channels, we characterized $\mu$1 modal behavior at the single-channel level. We found that the $\beta_1$-subunit did not create a new kinetic mode, but rather shifted the balance between two normally occurring modes to favor fast gating.

## MATERIALS AND METHODS

### Construction and transcription of plasmids

$\mu$1 and the *Xenopus* globin vector (pAlter-XG) were provided by Dr. J. Randall Moorman (University of Virginia) and the $\beta_1$-subunit by Dr. John W. Kyle (University of Chicago). $\mu$1 was provided with flanking 5′ and 3′ untranslated *Xenopus* globin sequences to improve the efficiency of expression in the *Xenopus laevis* oocyte system (Krieg and Melton, 1984).

The $\beta_1$-subunit was provided in the pAlter vector. To increase expression, $\beta_1$ was cloned into a vector in which 5′ and 3′ untranslated *Xenopus*

*Received for publication 31 July 1995 and in final form 8 March 1996.*
Address reprint requests to Dr. Steven Y. Chang, The University of Chicago, 5841 S. Maryland Avenue, MC 6094, Chicago, IL 60637. Tel.: 312-702-1481; Fax: 312-702-6789; E-mail: steve@hearts.bsd.uchicago.edu.
© 1996 by the Biophysical Society
0006-3495/96/06/2581/12 $2.00

globin sequences flanked the $\beta_1$-subunit sequence in a manner similar to that of $\mu$1. pAlter-XG was linearized with the restriction endonuclease *Bgl*II and subsequently treated with calf intestinal phosphatase to remove 5′ phosphate groups, thus preventing ligation of the cut ends. The $\beta_1$-subunit was cut out of pAlter with *Bam*HI, isolated via agarose gel electrophoresis, and then purified using 0.22 $\mu$M cellulose acetate Spin-X columns (Costar, Cambridge, MA). $\beta_1$ was then ligated into the *Bgl*II site of pAlter-XG. This was easily accomplished because the *Bgl*II and *Bam*HI digestions produced complementary fragments. RNA transcripts were synthesized in vitro with the mCAP mRNA Capping Kit (Stratagene, La Jolla, CA), using either T7 polymerase (supplied in the Stratagene kit) or SP6 polymerase (New England Biolabs, Beverly, MA), as determined by the promoter located upstream of the cDNA to be transcribed.

## Oocyte preparation and injection of cRNA transcript

Female *Xenopus laevis* frogs (NASCO, Ft. Atkinson, WI) were anesthetized by placing them in a solution of 0.15% tricaine methanesulfonate. Several lobes of ovary were removed and washed with $Ca^{2+}$-free OR-2+ (90 mM NaCl, 2.5 mM KCl, 1 mM $MgCl_2$, 5 mM HEPES, pH 7.6, 100 $\mu$g/ml gentamicin; Gibco-BRL, Grand Island, NY). The ovarian lobes were then manually teased apart and placed in $Ca^{2+}$-free OR-2+ containing 2 mg/ml collagenase (Sigma, St. Louis, MO). The oocytes were gently shaken for 45 min and rinsed again with $Ca^{2+}$-free OR-2+. The oocytes then underwent two more identical cycles of collagenase treatment. After enzymatic treatment, any remaining follicular cells were removed manually with a pair of fine-tipped forceps.

Stage V–VI oocytes were selected and injected with 50–100 ng of cRNA from a model 3-00-510-X 10-$\mu$l microinjector (Drummond Scientific Co., Broomall, PA). After 16–24 h of incubation in OR-2+ (90 mM NaCl, 2.5 mM KCl, 1 mM $CaCl_2$, 1 mM $MgCl_2$, 5 mM HEPES, pH 7.6, 100 $\mu$g/ml gentamicin, 50 units/ml nystatin; Sigma), oocytes were assayed for current by using two-electrode voltage clamping.

## Electrophysiological recording

Whole-oocyte $I_{Na}$ was measured by using a TEV-200 two-electrode voltage clamp (Dagan Corp., Minneapolis, MN) with a TEV-208 series resistance compensation circuit (Dagan Corp.), 16–24 h after injection of cRNA. The oocytes were placed in a flowing bath consisting of phosphate-free OR-2 (90 mM NaCl, 2.5 mM KCl, 1 mM $CaCl_2$, 1 mM $MgCl_2$, 5 mM HEPES, pH 7.6) in which voltage clamp records were obtained. The glass electrodes (World Precision Instruments, Sarasota, FL) were filled with 3 M KCl and had resistances of 0.5–1 M$\Omega$. $I_{Na}$ was filtered at 10 kHz and sampled at $\geq$25 kHz. $I_{Na}$ was acquired and analyzed with Axobasic 1.1. Oocytes with 4–6 $\mu$A of $I_{Na}$ were used for single-channel recordings, whereas oocytes with >6 $\mu$A of current were used for macropatch recordings. Gigaohm seals could be formed with a good success rate for up to 48 h after injection.

Single-channel and macropatch $Na^+$ currents were measured with an EPC-7 patch clamp (List Electronic, Darmstadt-Eberstadt, Germany). To obtain gigaohm seals on the oocyte membrane, the vitelline envelope was removed from the surface of the oocyte (Methfessel et al., 1986). This was accomplished by shrinking the oocyte in a hypertonic solution (consisting of 85 mg/ml of sucrose dissolved in OR-2+) so that the vitelline envelope separated from the membrane. The envelope was then easily removed with a pair of forceps. The oocytes were then placed in a depolarizing bath [120 mM potassium aspartate, 20 mM KCl, 1 mM $CaCl_2$, 1 mM $MgCl_2$, 10 mM HEPES, pH 7.6 (for cell-attached single-channel recordings); or 120 mM potassium aspartate, 20 mM KCl, 1 mM $MgCl_2$, 10 mM EGTA, 10 mM HEPES, pH 7.4 (for cell-attached or inside-out macropatch recordings)] so that the oocyte membrane would rest at ~0 mV. Soft glass (Drummond Scientific Co.) patch pipettes were filled with either 280 mM NaCl, 1 mM $CaCl_2$, 1 mM $MgCl_2$, 10 mM tetraethylammonium-Cl, 10 mM HEPES, pH 7.6 (280 mM $Na^+$ solution) for single-channel recordings or 140 mM NaCl, 1 mM $CaCl_2$, 1 mM $MgCl_2$, 10 mM TEA-Cl, 10 mM HEPES, pH 7.6 (140 mM $Na^+$ solution) for macropatch recordings. Single-channel currents were filtered at 3 kHz (−3 dB) and sampled at 12.5 kHz, whereas macropatch currents were filtered at 5 kHz (−3 dB) and sampled at 50 kHz, all with 66-ms voltage steps. Single-channel experiments were performed at room temperature (20–22°C), whereas macropatch data were collected either at room temperature or at 12°C. A Physitemp TS-4 (Sensortek, Clifton, NJ) was used to lower the bath temperature to 12°C. Patch-clamp data acquired with Axobasic 1.1 were analyzed with a custom program written and supplied by David Piper (Webfoot Software, University of Utah, Salt Lake City). Analog capacity compensation was achieved with the circuitry of the EPC-7, and any remaining capacitance was compensated either by subtracting averages of traces without channel activity in the case of single-channel recordings or by using the P/4 method of Bezanilla and Armstrong (1977) in the case of macropatch recordings.

Depolarizing step frequency for single-channel recordings was 0.33 Hz. The main reasons for allowing 3 s between pulses were: 1) to allow channels to return to steady state, and 2) to obtain enough data for analysis. Based on recovery from inactivation data (Satin et al., 1992), interpulse intervals ought to be 20 s, but this would not have allowed for enough single-channel data to be obtained for analysis, because patches generally did not last for more than 90 min, most often lasting for less than 30 min. Interpulse intervals for macropatches were set at either 0.300 s or 20 s to favor either the fast mode or the slow mode, respectively, as explained in the Results. Based on two-electrode voltage-clamp steady-state inactivation curves, the holding potential was set at −100 mV to allow for complete availability during experiments.

## Open-time histograms

Histograms of open times at test potentials of −40 mV, −20 mV, and 0 mV were fit individually with Discrete (Provencher, 1976), a fitting routine with a basis in the Fourier convolution theorem. Furthermore, open times at each potential were combined into a single set at each test potential and fit with Discrete to assess the consistency of our results. Because the patches generally contained more than one channel, open times were measured only for those segments without overlapping openings to eliminate any ambiguity about times at which channels closed. Openings were detected with the half-amplitude threshold method of Colquhoun and Sigworth (1983), and channel amplitude was determined with Patlak's (1988) variance-mean analysis method. When the open-time histograms were fitted, the first bin was ignored to minimize errors in the fitting process. The bin width was 80 $\mu$s. The histograms were fit with the following equation:

$$c(t) = [\mathrm{Amp_f} * \exp(-t/\tau_f)] + [\mathrm{Amp_s} * \exp(-t/\tau_s)], \quad (1)$$

where $c(t)$ is counts per 80-$\mu$s bin, $\mathrm{Amp_f}$ is the amplitude of the fast component, $\tau_f$ is the time constant of the fast component, $\mathrm{Amp_s}$ is the amplitude of the slow component, $\tau_s$ is the time constant of the slow component, and $t$ is time. A filter frequency of 3 kHz resulted in a calculated dead time ($T_d$) of 60 $\mu$s, and the measured $T_d$ for the patch-clamp apparatus was 75 $\mu$s when we filtered at 3 kHz and sampled at 12.5 kHz.

## Control studies

Coexpression of the $\beta_1$-subunit with $\mu$1 in oocytes did not affect the single-channel slope conductance of the $\alpha$-subunit channels (data not shown). The conductance for both $\mu$1 alone ($n$ = 8 to 13 patches, depending on the test potential) and $\mu$1 + $\beta_1$ ($n$ = 5 to 7 patches) was 39 pS with a patch pipette solution containing the 280 mM $Na^+$ solution. With the 140 mM $Na^+$ solution the slope conductances of $\mu$1 ($n$ = 5) and $\mu$1 + $\beta_1$ ($n$ = 5) were identical at 26 pS.

A representative $NP_o$ history for $\mu$1 alone (Fig. 1 *C*, patch p30715b) shows that with 3-s interpulse intervals, both fast and slow gating behavior occurred throughout the entire 1345 sweeps and that the frequency of high

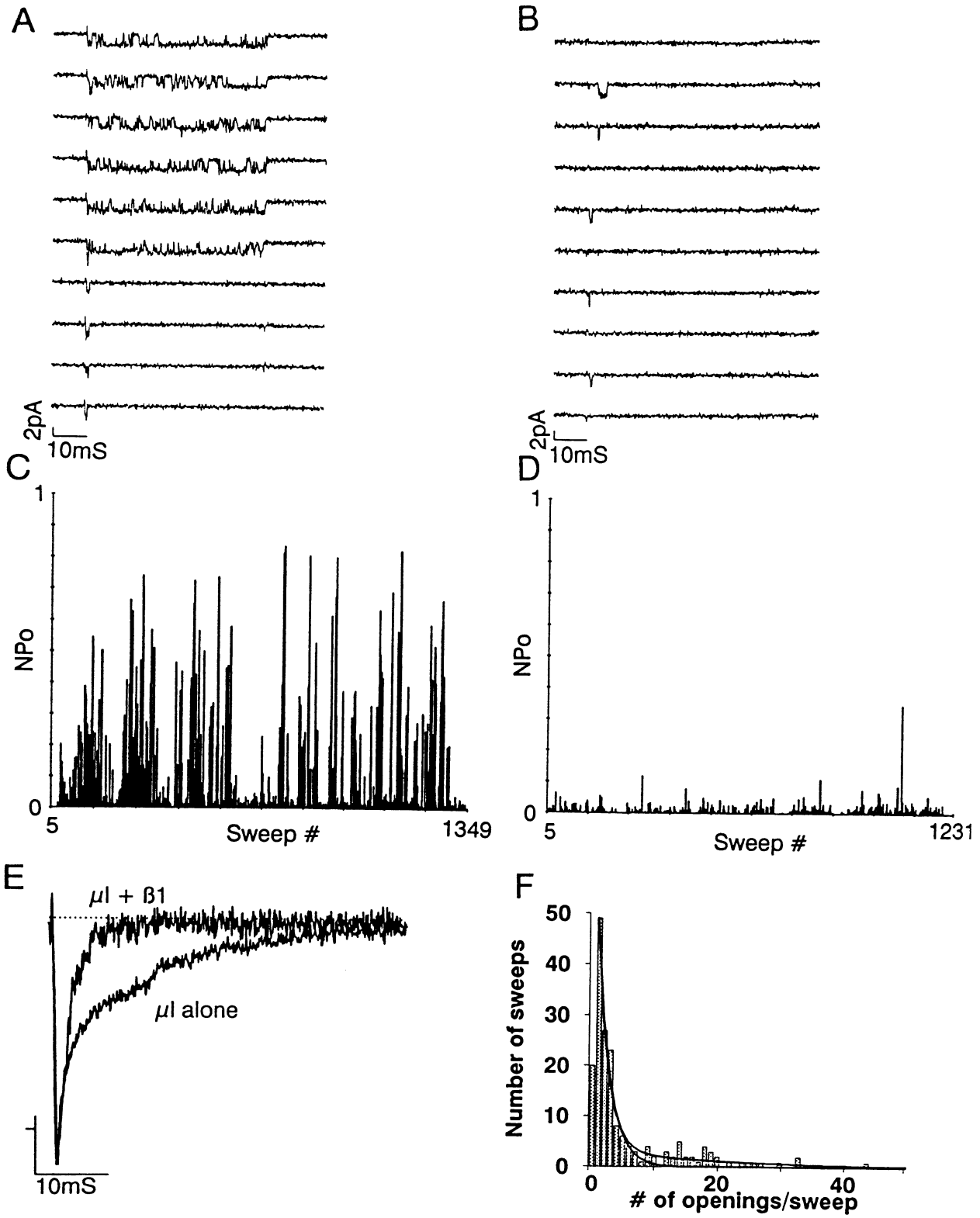


FIGURE 1 The $\beta_1$-subunit favors fast mode kinetics. Ten consecutive and representative sweeps for (*A*) $\mu 1$ alone (patch p30715b) and (*B*) $\mu 1 + \beta_1$ (patch p30713a) at a test potential of $-20$ mV. Single-channel events were $-2.3$ pA and $-2.5$ pA, respectively. A maximum of three overlapping events were detected in 1345 sequential sweeps for $\mu 1$ alone, and a maximum of two overlapping events were detected in 1226 sweeps for $\mu 1 + \beta_1$. (*C* and *D*) $NP_o$ histories for the same patches as seen in *A* and *B*, respectively. Note the nonrandom distribution of high and low $P_o$ sweeps for $\mu 1$ alone (*C*). Coexpression of $\beta_1$ eliminated high $P_o$ sweeps (*D*). (*E*) Ensemble averages for $\mu 1$ alone (same patch as *A*) and $\mu 1 + \beta_1$ (same patch as *B*). (*F*) The histogram of the number of openings per sweeps required a two-exponential function for best fit of $\mu 1$ alone (patch contained a maximum of five overlapping events in 197 sequential sweeps) and was fit with Eq. 3. The two-exponential fit parameters were $Amp_1 = 81.7$, $k_1 = 1.79$, $Amp_2 = 3.4$ and $k_2 = 18.9$. Single-fit parameters were Amp = 78.5 and $k = 2.08$. Depolarizing step frequency to $-20$ mV was 0.33 Hz for all patches depicted in this figure.

$NP_o$ sweeps remained fairly constant during the recording period. In 9 of 13 patches ranging from 300 to 1587 sweeps, there was minimal diminution of slow-mode behavior at a 0.33-Hz step frequency when stepping to either −20 or 0 mV. Kinetic stability was evaluated by examining the fraction of null sweeps, sweeps with a $P_o \leq 0.050$, and sweeps with a $P_o > 0.050$ in the first and last 100 sweeps in five patches in which the test potential was −20 mV. At −20 mV, the fraction of sweeps with a $P_o > 0.050$ in the initial 100 sweeps was 0.234, and in the last 100 sweeps it was 0.240. Similarly, in four patches at 0 mV, the fraction of sweeps with a $P_o > 0.050$ was 0.137 in the first 100 sweeps and 0.100 in the final 100 sweeps. The other four patches demonstrated some reduction in slow-mode behavior during the recording period at −20 mV or 0 mV. Patches in which $\beta_1$ was coexpressed with $\mu$1 demonstrated little variability in channel opening behavior (Fig. 1 *D*).

## RESULTS

### Modal behavior

Representative sequential sweeps for $\mu$1 alone and $\mu$1 + $\beta_1$, respectively, are shown in Fig. 1, *A* and *B*. $\mu$1 alone (Fig. 1 *A*) demonstrates sweeps with single openings (low $P_o$ sweeps), nonrandomly interspersed with sweeps with bursts (high $P_o$ sweeps). Coexpression of the $\beta_1$-subunit with $\mu$1 resulted in elimination of the high $P_o$ gating pattern, so that behavior of $\mu$1 + $\beta_1$ showed only single, short openings occurring early in the depolarizing pulse similar to that of native channels (Sigworth and Neher, 1980; Weiss and Horn, 1986). The behavior of $\mu$1 + $\beta_1$ appeared to be similar to the low $P_o$ sweeps of $\mu$1 alone (compare Fig. 1 *B* with the last four sweeps of Fig. 1 *A*). (The low $P_o$ mode will be called the "fast" mode, and the high $P_o$ mode will be called the "slow" mode.) The representative $NP_o$ history for $\mu$1 alone (Fig. 1 *C*) demonstrates more clearly the nonrandom clustering of high and low $NP_o$ sweeps. The current traces and the $NP_o$ history for $\mu$1 + $\beta_1$ (Fig. 1, *B* and *D*) show that high $NP_o$ sweeps were virtually eliminated when $\beta_1$ was coexpressed with the $\alpha$-subunit in *Xenopus* oocytes.

The ensemble currents of $\mu$1 alone and $\mu$1 + $\beta_1$ were scaled for easy comparison of current shape. The ensemble for $\mu$1 alone shows fast and slow components for $I_{Na}$ decay, whereas the ensemble average for $\mu$1 + $\beta_1$ demonstrates predominantly fast $I_{Na}$ decay (Fig. 1 *E*). The slow decay component for the $\mu$1 alone ensemble is not as large as seen with two-electrode voltage-clamp $I_{Na}$ or with macropatch $I_{Na}$, probably because the short interpulse intervals of 3 s may favor the fast mode (see below).

A histogram of the number of openings per sweep was constructed for a representative patch of $\mu$1 alone (Fig. 1 *F*). An exponential fit of this distribution required two components in which $Amp_1 = 81.7$, $k_1 = 1.79$ openings per sweep, $Amp_2 = 3.4$, and $k_2 = 18.9$ openings per sweep. This result further suggests two alternative gating schemes in which channels open an average of 1–2 times or an average of 20 times during each depolarizing step. Fits of histograms of number of openings per sweep for seven other $\mu$1 patches yielded similar results, consistent with the presence of at least two gating schemes. Similar analysis of four patches with $\mu$1 + $\beta_1$ yielded histograms that were best fit by a single exponential, suggesting the predominance of only a single gating scheme in which openings only occur once or twice.

### Mean open times

If bursting behavior and discrete openings are associated with different exit rates from the open state, then each should be associated with a different mean open time. Mean open times (MOTs) were determined for each patch and for all patches together. The pooled histograms were best fit with two exponentials for both $\mu$1 and $\mu$1 + $\beta_1$ at −40, −20, and 0 mV, a result typically interpreted as indicating two kinetic populations of channels. With a test potential of −40 mV, the pooled open-time histograms for both $\mu$1 ($n$ = 6) and $\mu$1 + $\beta_1$ ($n$ = 6) were best fit with two exponentials, resulting in MOTs of 0.26 ms and 0.68 ms for $\mu$1 and 0.28 ms and 0.56 ms for $\mu$1 + $\beta_1$. Fitting the pooled open time histograms at a test potential of −20 mV resulted in MOTs of 0.39 ms and 1.25 ms for $\mu$1 ($n$ = 8) and 0.44 ms and 1.25 ms for $\mu$1 + $\beta_1$ ($n$ = 5) (Fig. 2, *A* and *B*). Finally, at 0 mV, the pooled open-time histograms yielded MOTs of 0.30 ms and 1.99 ms for $\mu$1 ($n$ = 10) and a single MOT of 0.32 ms for $\mu$1 + $\beta_1$ ($n$ = 5). The fact that the two MOTs at each respective potential were identical whether or not $\beta_1$ was coexpressed with $\mu$1 suggests that the two open states for $\mu$1 and $\mu$1 + $\beta_1$ are identical. The major effect of $\beta_1$-subunit coexpression was reduction in the ratio of the amplitudes of the long MOT component to short MOT component. To ensure that the two MOT components were not a consequence of pooling of data from multiple patches, the individual patch histograms were analyzed for voltage steps of −40 mV, −20 mV, and 0 mV. At −40 mV only one exponential component could be detected, with an average MOT of 0.29 ± 0.02 ms (mean ± SEM; $n$ = 6) for $\mu$1 alone and 0.35 ± 0.05 ms for $\mu$1 + $\beta_1$ ($n$ = 6). At −20 mV two exponential components could be distinguished, with MOTs of 0.44 ± 0.04 ms and 1.47 ± 0.17 ms for $\mu$1 alone ($n$ = 8) and 0.49 ± 0.03 and 1.50 ms for $\mu$1 + $\beta_1$ ($n$ = 5). At 0 mV two components were seen, with MOTs of 0.29 ± 0.03 ms and 2.03 ± 0.14 ms for $\mu$1 alone ($n$ = 10) and 0.36 ± 0.09 ms and 2.12 ms for $\mu$1 + $\beta_1$ ($n$ = 5). In each case only one of the individually fit histograms at −20 mV or 0 mV for $\mu$1 + $\beta$1 showed two exponentials. These comparisons support the impression from the pooled data that the fast and slow MOT components are the same with or without coexpression of the $\beta_1$-subunit, but that the slow component is more difficult to detect in a single patch in the presence of the $\beta_1$-subunit. The voltage dependence of the two MOT values with and without $\beta_1$ coexpression is shown in Fig. 3.

If the two populations of MOTs represent different kinetics of the two modes, then it should be possible to associate the fast mode with the short MOT population and the slow mode with the long MOT population. Delcour and Tsien (1993) and Delcour et al. (1993) studied kinetic modal behavior of N-type $Ca^{2+}$-channels by using differences in

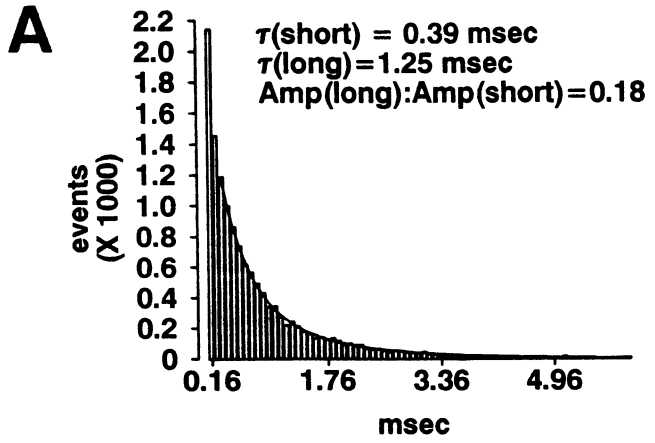


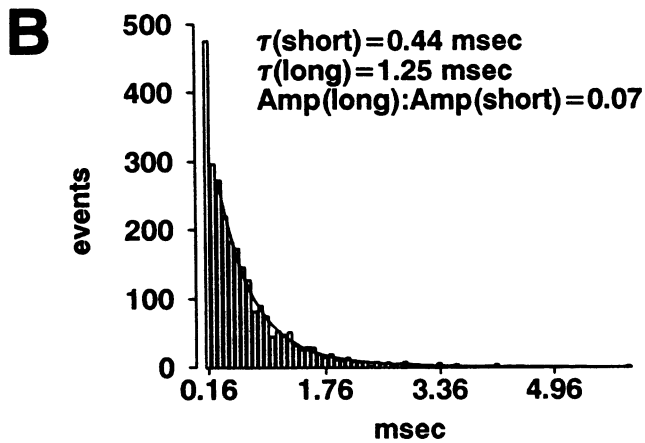


FIGURE 2 $\mu 1$ and $\mu 1 + \beta_1$ have identical open times. (*A*) The pooled open time histogram for $\mu 1$ alone was best fit with two exponentials resulting in MOTs of 0.39 ms and 1.25 ms at a test potential of −20 mV. (*B*) The pooled open time histogram for $\mu 1 + \beta_1$ was also best fit with two exponentials for MOTs of 0.44 ms and 1.25 ms at −20 mV. The ratio of the amplitudes of the long to short components is larger for $\mu 1$ alone (0.18) than for $\mu 1 + \beta_1$ (0.07). Histograms were fit to Eq. 1, and bin widths were 80 $\mu$s. Data for −40 and 0 mV are not shown.

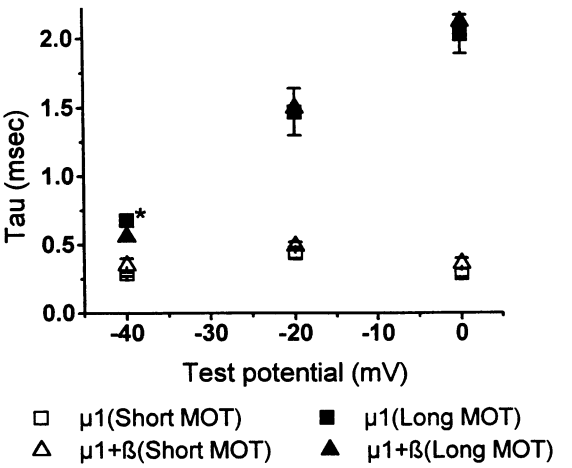


FIGURE 3 Individually fit open time histograms for both $\mu 1$ and $\mu 1 + \beta_1$ demonstrate the same open times at −40, −20, and 0 mV. Significant differences were found when comparing the long MOT of either $\mu 1$ or $\mu 1 + \beta_1$ with the short MOT of the corresponding channel ($p < 0.010$) at each test potential. Actual MOT values are found in the text. The asterisk indicates data points derived from the summed open time histograms, because long MOTs at −40 mV were difficult to detect. Vertical bars are standard errors of the mean.

the probability of opening ($P_o$) to separate the different modes. This method of analysis was used to separate the two modes manifested by $\mu 1$. We therefore tested the following criteria. The sweep was assigned to the fast mode when $P_o \leq 0.010$, allowing 0.66 ms of cumulative open time and and effectively excluding the slow mode with a putative MOT of 1.5 ms. The sweep was assigned to the slow mode when $P_o \geq 0.200$, requiring at least 13.2 ms of cumulative open time and including most of the slow-mode bursts. The $NP_o$ of each sweep was divided by the maximum number of overlaps ($N$) found in the data set from which that sweep originated to determine $P_o$ because the patches contained between one and five channels, allowing coexistence of two types of behavior in a single depolarizing sweep. When $0.010 < P_o < 0.200$, both the slow mode and fast mode could be detected in multichannel patches, and the MOT histogram showed two exponential time constants not different from the low $P_o$ and the high $P_o$ data. It therefore appears that the sampling method did not distort the MOT values. When we examined open times for sweeps with $P_o \leq 0.010$ or $P_o \geq 0.200$, the open-time histograms were best fit with a single exponential. Pooled histograms at each potential were required because of the limited number of events as a consequence of these strict criteria. The MOTs when $P_o \leq 0.010$ and when $P_o \geq 0.200$ resembled the MOTs obtained when open times for all sweeps at each respective test potential were examined in histograms of pooled open times. For example, the mean open time for $\mu 1$ alone at −20 mV was 0.35 ms for sweeps with $P_o \leq 0.010$, whereas the MOT for sweeps with $P_o \geq 0.200$ was 1.1 ms (Fig. 4, *A* and *B*). Compare this to the pooled open-time histogram for $\mu 1$, which was best fit with MOTs of 0.39 and 1.25 ms at −20 mV (Fig. 2 *B*). The MOT, at 0 mV, for $\mu 1$ alone was 0.33 ms for sweeps with $P_o < 0.010$ and 1.6 ms for sweeps with $P_o > 0.200$, whereas the pooled open-time histogram was best fit with MOTs of 0.30 and 1.99 ms (data not shown). In summary, the shorter MOTs at each potential were associated with the fast gating mode, whereas the longer MOTs at each potential were associated with the bursting, slow gating mode. This same type of analysis could not be performed with $\mu 1 + \beta_1$ because of the rarity of burst behavior. It should be noted again that the short MOT of $\mu 1$ alone and the MOT of $\mu 1 + \beta_1$ appear to be identical, implying that the gating scheme of the fast mode of $\mu 1$ is equivalent to that of $\mu 1 + \beta_1$.

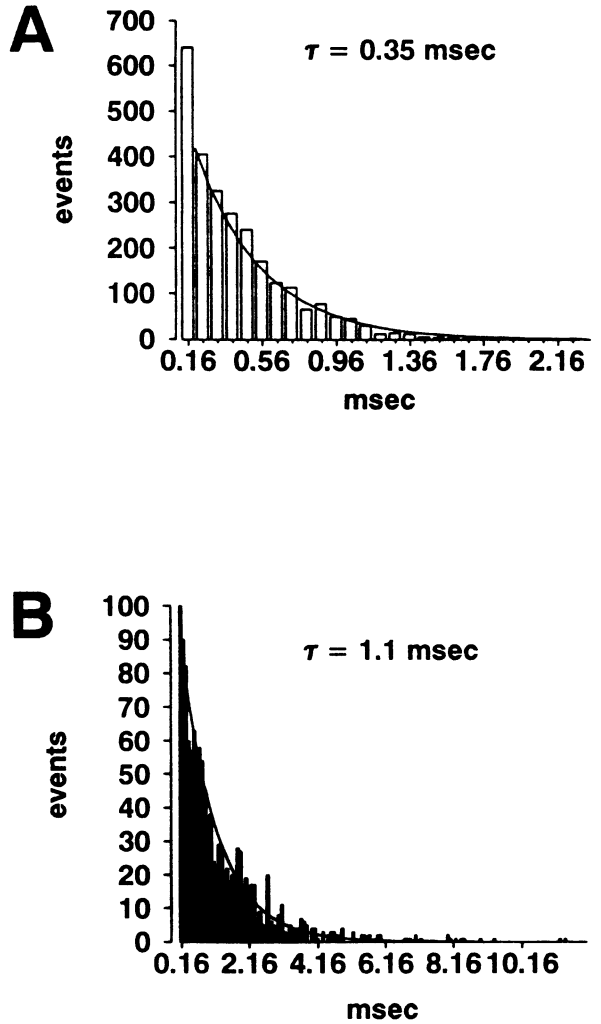


FIGURE 4 Open times for fast mode ($P_o \leq 0.010$) and slow mode ($P_o \geq 0.200$) of $\mu$1 are identical to the open times for all sweeps in pooled open-time histograms. Open times for sweeps with $P_o \leq 0.010$ were best fit with a single exponential of 0.35 ms at a test potential of −20 mV, whereas open times for sweeps with $P_o \geq 0.200$ were best fit with a single exponential of 1.1 ms, also at −20 mV. These open times closely corresponded with those derived from the pooled open-time histograms at −20 mV, where the open times were 0.39 ms ($\mu$1), 0.44 ms ($\mu$1 + $\beta_1$), and 1.25 ms (both $\mu$1 and $\mu$1 + $\beta_1$).

## Frequency dependence of modal behavior

Even in the absence of the $\beta_1$ subunit the $\mu$1 channel appears to spend most of its time in the fast mode at a depolarizing frequency of 0.33 Hz. To examine the issue of the frequency dependence of modal behavior, oocyte-attached macropatches of $\mu$1 were obtained and currents were examined with a holding potential of −100 mV, and test potentials varied from −30 mV to 0 mV in 10-mV increments. By varying the interpulse interval, either fast or slow gating could be favored. The first current of the train after a long pause always demonstrated the characteristic slow inactivation. When step depolarizations were applied every 20 s, slow gating of $\mu$1 was seen, as evidenced by slow $I_{Na}$ decay (Fig. 5 *A*). When depolarizing at the relatively rapid rate of 3.3 Hz, fast gating behavior of $\mu$1 alone was observed, as evidenced by rapid decay of $I_{na}$ at steady state. Peak $I_{Na}$ during rapid pulsing was generally less than peak $I_{Na}$ during slow pulsing within a given patch. It would seem that the rapid depolarizations favored the fast gating mode, whereas slow pulse trains allowed the channels to remain in the slow mode.

Macropatches of $\mu$1 + $\beta_1$ were obtained under identical conditions. $I_{Na}$ decay for $\mu$1 + $\beta_1$ was always rapid whether step frequency was 3.3 Hz or 0.05 Hz. Peak $I_{Na}$ did not decrease when the $\beta_1$ subunit was coexpressed with $\mu$1 during rapid pulsing. This was evidenced by the fact that ensemble-averaged peak $I_{Na}$ from the same patch was the same whether interpulse intervals were 300 ms or 20 s (Fig. 5 *B*). Furthermore, comparison of $\mu$1 + $\beta_1$ current traces with current traces of $\mu$1 during rapid pulsing shows that the shapes of these currents are not significantly different (Fig. 5 *C*). That is, the $I_{Na}$ of the fast mode of $\mu$1 alone looks like the $I_{Na}$ of $\mu$1 + $\beta_1$, supporting the idea that the gating kinetics of $\mu$1 + $\beta_1$ and the fast mode of $\mu$1 alone are identical.

## Voltage dependence of mode shifting

Single-channel studies were performed to determine whether modal gating was affected by different holding potentials (Hebert et al., 1994; Ji et al., 1994). Seven cell-attached gigaohm patches containing 3–8 channels were obtained, and $V_{hold}$ was varied from −100 mV to −80 mV, then to −60 mV, with 150 or 300 depolarizing pulses to −20 mV at each holding potential. Interpulse intervals were 3 s, and interpotential intervals were approximately 1–3 min. A holding potential of −120 mV was then applied if the oocyte membrane could withstand such a hyperpolarized holding potential. In the four cases in which −120 mV could be maintained, channel behavior closely matched that at −100 mV, so "run-down" was not a major factor. In another case in which the holding potential was returned to −100 mV from a holding potential of −60 mV, channel behavior was also restored. Qualitatively, a consistent behavioral pattern was identified. With more depolarized holding potentials, bursting occurred with less frequency, and fast mode behavior predominated (Fig. 6). This is consistent with the idea that fast modal gating is favored at more depolarized holding potentials (Hebert et al., 1994) or that depolarization has a greater effect on recovery for the slow mode.

## Time-to-peak $I_{Na}$

Time to peak $I_{Na}$ was too rapid to resolve at 22°C, so the temperature was lowered in inside-out macropatches to 12°C to examine current kinetics. For $\mu$1 alone, fast gating modes were favored by rapid depolarizing pulses (interpulse intervals of 0.300 s), and slow gating modes were favored

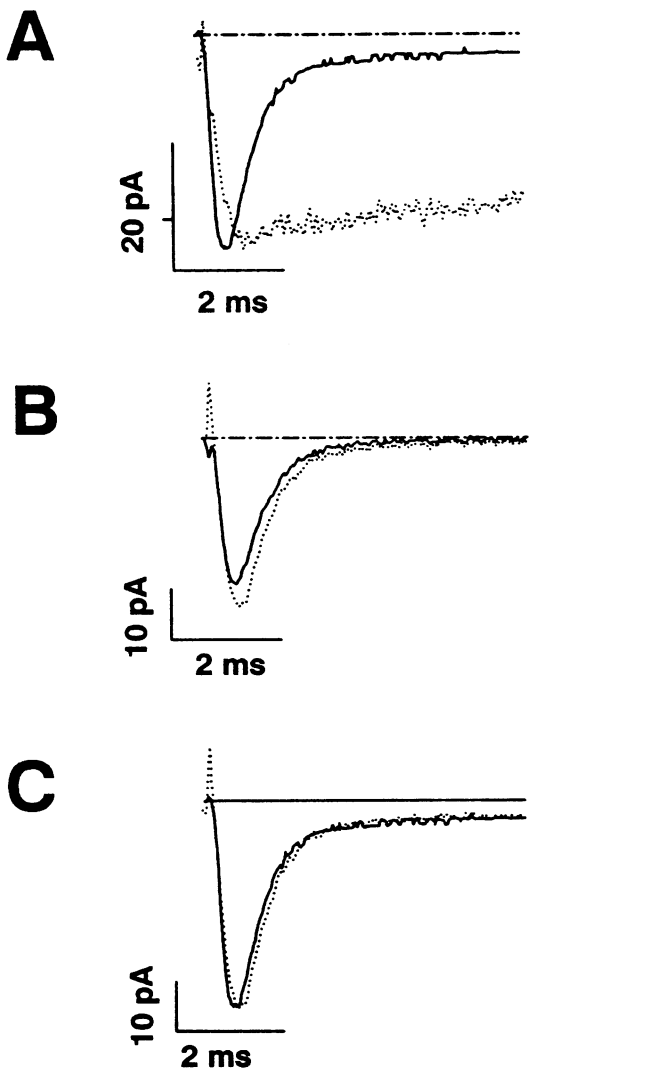


FIGURE 5 (*A*) The fast mode of $\mu 1$ is favored by rapid depolarizations at 3.3 Hz, whereas the slow mode of $\mu 1$ is favored by an extremely slow depolarization rate of 0.05 Hz. Fast-mode behavior is represented by rapid $I_{Na}$ decay, whereas slow-mode behavior is represented by slow $I_{Na}$ decay. (*B*) When the $\beta_1$-subunit is coexpressed with $\mu 1$, rapid $I_{Na}$ decay occurs, regardless of depolarization frequency, and peak $I_{Na}$ remains constant, even during rapid test steps. Whether the interpulse intervals were 300 ms or 20 s, the ensemble-average peak current and $I_{Na}$ are identical, indicating that $\beta_1$ favors the fast mode. (*C*) Fast modal gating of $\mu 1$ demonstrates kinetics identical to that of $\mu 1 + \beta_1$. Direct comparison of the macropatches of $\mu 1 + \beta_1$ and macropatches in which depolarization frequency was high (3.3 Hz) shows that $\mu 1 + \beta_1$ and the fast mode are identical. These data were collected at 22°C in cell-attached macropatches with a $V_{hold}$ of −100 mV and a $V_{test}$ of −20 mV. $I_{Na}$ at −30, −10, and 0 mV behaved in a similar manner.

by slow depolarizing pulses (every 20 s). For $\mu 1 + \beta_1$, pulses were applied every 20 s so as not to bias rapid gating via pulse frequency. Unlike Fleig et al. (1994), we did not see irreversible shifts to fast mode gating with time after excision of the patches.

As can be seen in Fig. 7 *A*, the time to peak $I_{Na}$ at 12°C appeared to be more rapid for the fast mode than for the slow mode at −20 mV when the holding potential was −100 mV. The same phenomenon was seen at 0 mV (data not shown). In contrast, times to peak for the fast mode and $\mu 1 + \beta_1$ are identical (Fig. 5 *C*), so it can be concluded that the time to peak $I_{Na}$ for $\mu 1 + \beta_1$ is also faster than for the slow mode of $\mu 1$ alone. However, the time course of the current is significantly influenced by channel open time, and these are longer for the slow mode (Fig. 3). That is, with delayed O → I transitions, time to peak would be longer than if O → I rates were increased. To determine whether it is possible to obtain a delayed time to peak current with identical activation pathways and different MOTs, we simulated $I_{Na}$ with the CSIM modeling program (Axon Instruments, Foster City, CA) using activation rate constants based on those obtained by Scanley et al. (1990) for canine cardiac Purkinje cells at a test potential of −42 mV. The following kinetic scheme was used:

$$R(1) \leftrightarrow C(2) \leftrightarrow C(3) \leftrightarrow O(4)$$
$$\searrow \swarrow$$
$$I(5)$$

$I_{Na}$ was modeled for both $\mu 1$ alone and $\mu 1 + \beta_1$, assuming that the activation pathways were identical. That is, the rate constants for $R_1 \leftrightarrow R_2 \leftrightarrow C_3 \leftrightarrow O_4$ and $C_3 \rightarrow I_5$ for $\mu 1$ and $\mu 1 + \beta_1$ were assumed to be identical. The rate constants for the $O_4 \rightarrow I_5$ ($k_{oi}$) transitions were varied to produce open times appropriate for $\mu 1$ alone and $\mu 1 + \beta_1$ at a test potential of −20 mV. The rate constant for the $O_4 \rightarrow C_3$ ($k_{oc}$) transition remained invariant at 666 transitions/s, whereas $k_{oi}$ was set at 1 transition/s for $\mu 1$ alone and 1334 transitions/s for $\mu 1 + \beta_1$. This allowed for MOTs of 1.5 ms for $\mu 1$ alone and 0.5 ms for $\mu 1 + \beta_1$ in the simulation, matching the measured MOTs for $\mu 1$ and $\mu 1 + \beta_1$ at −20 mV. CSIM was used to generate 3000 single-channel sweeps based on the rate constants for $\mu 1$ with and without $\beta_1$. To mimic actual recording conditions, filter frequency was 3 kHz, sample frequency was 12.5 kHz, and root mean square noise was 0.200 pA. The simulated data were analyzed in the same manner as acquired data. Ensemble averages of the simulated data closely resemble ensemble averages of true data, showing that time to peak $I_{Na}$ can be different simply because of differences in mean open times (Fig. 7 *B*). These model results demonstrate that it is indeed possible to see faster time to peak $I_{Na}$ with identical activation pathways without ruling out the possibility that activation pathways are different for the different modes and when the $\beta_1$-subunit is coexpressed.

## First latencies

A misleading estimate of activation from time to peak current can be avoided by direct measurement of first latencies. This requires analysis of single-channel patches to avoid the ambiguity of different modes within a single patch. Four single-channel patches were obtained, two of which had enough data at −20 mV for kinetic estimates of first latencies. One of the patches was of $\mu 1$ alone and the

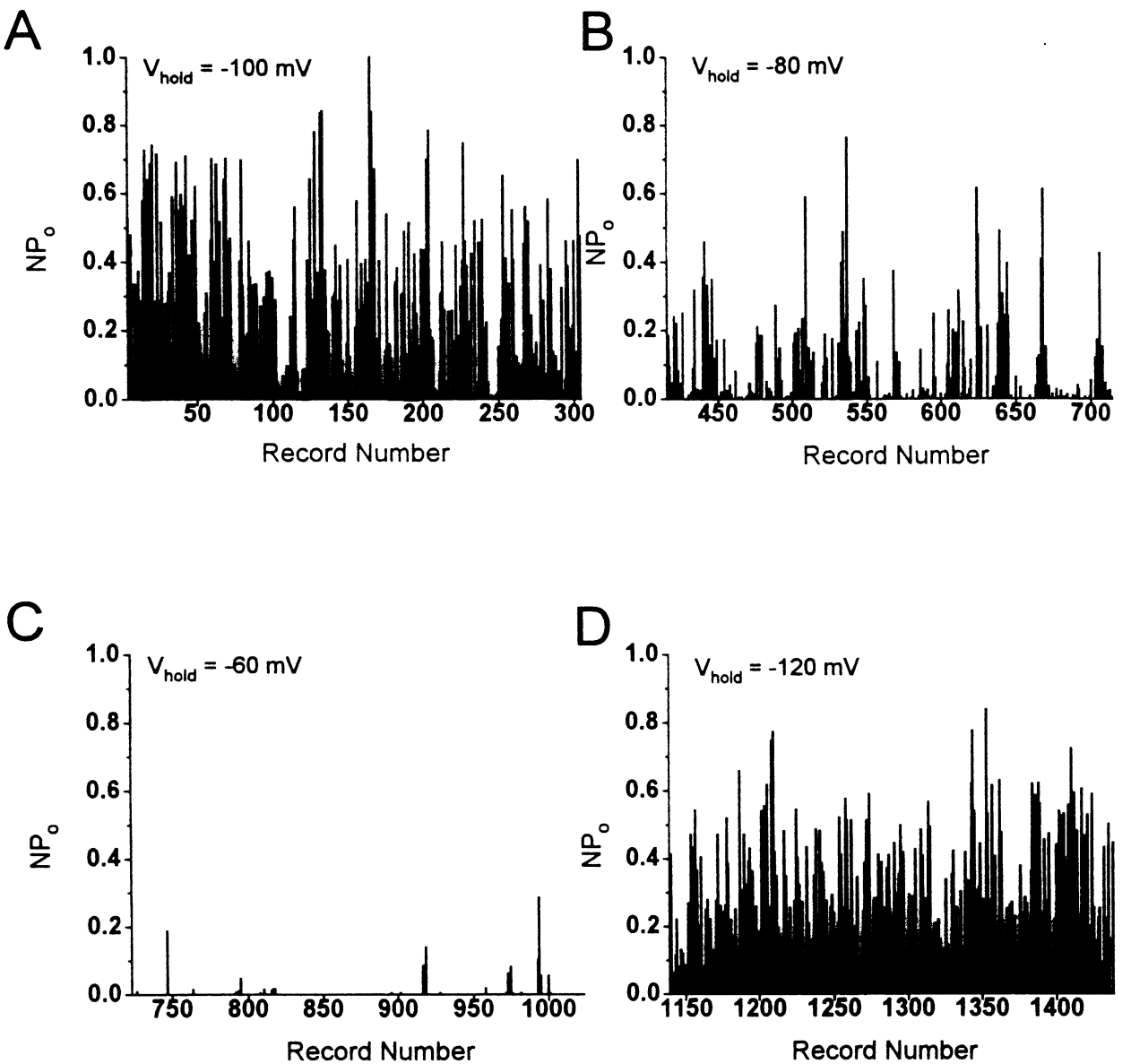


FIGURE 6 Fast-mode gating is favored by more depolarized holding potentials. (*A*) At a holding potential of −100 mV, $\mu$1 gating demonstrates both fast and slow modes. (*B*) When holding at −80 mV, slow-mode gating was diminished, whereas fast-mode gating continued. (*C*) When the holding potential was −60 mV, $\mu$1 gating was exclusively fast. (*D*) Stepping back to −120 mV restored the slow mode. $V_{test}$ was always −20 mV in these experiments.

other was of $\mu 1 + \beta_1$. The $\mu$1 alone patch lasted for 452 sweeps, and the $\mu 1 + \beta_1$ patch lasted for 600 sweeps.

First latencies were examined in several ways. First, the first latency for $\mu 1 + \beta_1$ was compared with the first latency for the slow mode of $\mu$1 alone. Second, the first latency for the fast mode of $\mu$1 was compared with the first latency for the slow mode of $\mu$1. Finally, the first latency for $\mu 1 + \beta_1$ was compared with the first latency for the fast mode of $\mu$1 alone. The time for first latency to reach half-maximum ($t_{1/2}$) was used as a measure of activation (Zhou et al., 1991; Böhle and Benndorf, 1995). All 600 sweeps of the $\mu 1 + \beta_1$ patch were used to generate a first latency curve. To obtain first latency curves for the fast mode of $\mu$1 and the slow mode of $\mu$1, sweeps were separated via $P_o$ criteria. If sweeps had a $P_o \leq 0.010$, they were classified as fast mode, and these sweeps were used to generate the first latency curve for the fast mode of $\mu$1 alone. If sweeps had a $P_o \geq 0.200$, they were classified as slow mode, and these sweeps were used to generate the first latency curve for the slow mode of $\mu$1 alone. With only one channel in the patch, no contamination of mixed modes could occur unless mode shift occurred during the step before the channel inactivated. The $t_{1/2}$ for $\mu 1 + \beta_1$ was 450 $\mu$s, whereas the $t_{1/2}$ for the fast mode of $\mu$1 was 400 $\mu$s. The $t_{1/2}$ for the slow mode of $\mu$1 was 700 $\mu$s. These comparisons show that $\mu 1 + \beta_1$ activates more quickly than the slow mode of $\mu$1 alone, and that the fast mode of $\mu$1 alone activates more rapidly than the slow mode of $\mu$1 alone.

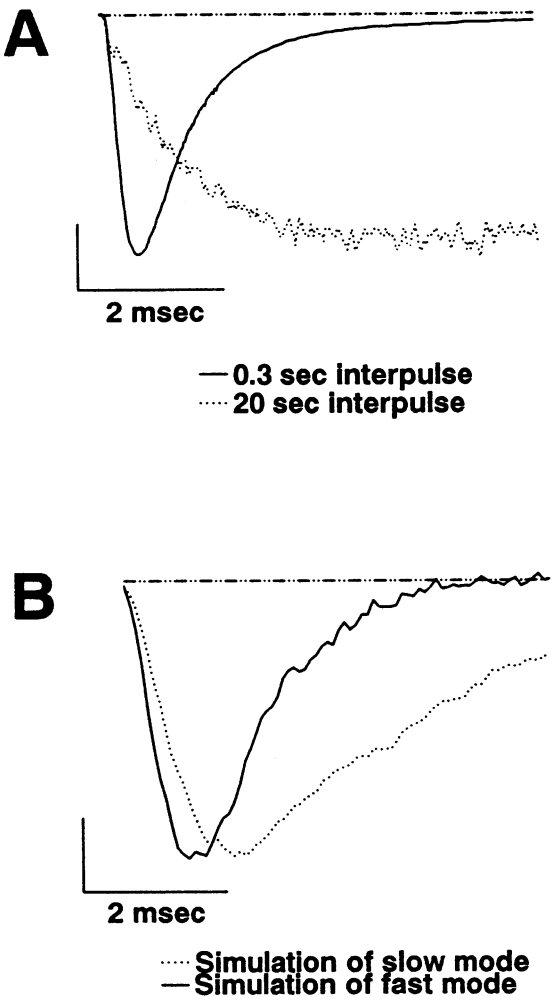


FIGURE 7 (*A*) Fast-mode gating of $\mu 1$ demonstrates a more rapid time to peak $I_{Na}$ than does slow-mode gating. The fast mode was favored by rapid depolarizations, whereas the slow mode was favored by a slow depolarizing step frequency. These inside-out macropatches were collected at 12°C to enhance resolution of time to peak $I_{Na}$. The holding potential was −100 mV and test potential was −20 mV. (*B*) The time to peak $I_{Na}$ can be altered simply by altering the O → I rate constant to match MOTs measured experimentally, as shown in this simulation. A different time to peak $I_{Na}$ does not necessarily mean that the activation pathways for $\mu 1$ and $\mu 1 + \beta_1$ are different. $k_{O4I5} = 1$ for $\mu 1$ (or the slow mode), whereas $k_{O4I5} = 1334$ for $\mu 1 + \beta_1$ (or the fast mode of $\mu 1$). All other rate constants were identical for $\mu 1$ and $\mu 1 + \beta_1$. $k_{R1R2} = 7734$, $k_{R2R1} = 0.001$, $k_{R2C3} = 4290$, $k_{C3R2} = 0.001$, $k_{C3O4} = 640$, $k_{O4C3} = 666$, $k_{C3I5} = 960$, $k_{I5C3} = 0.001$, and $k_{I5O4} = 0.001$.

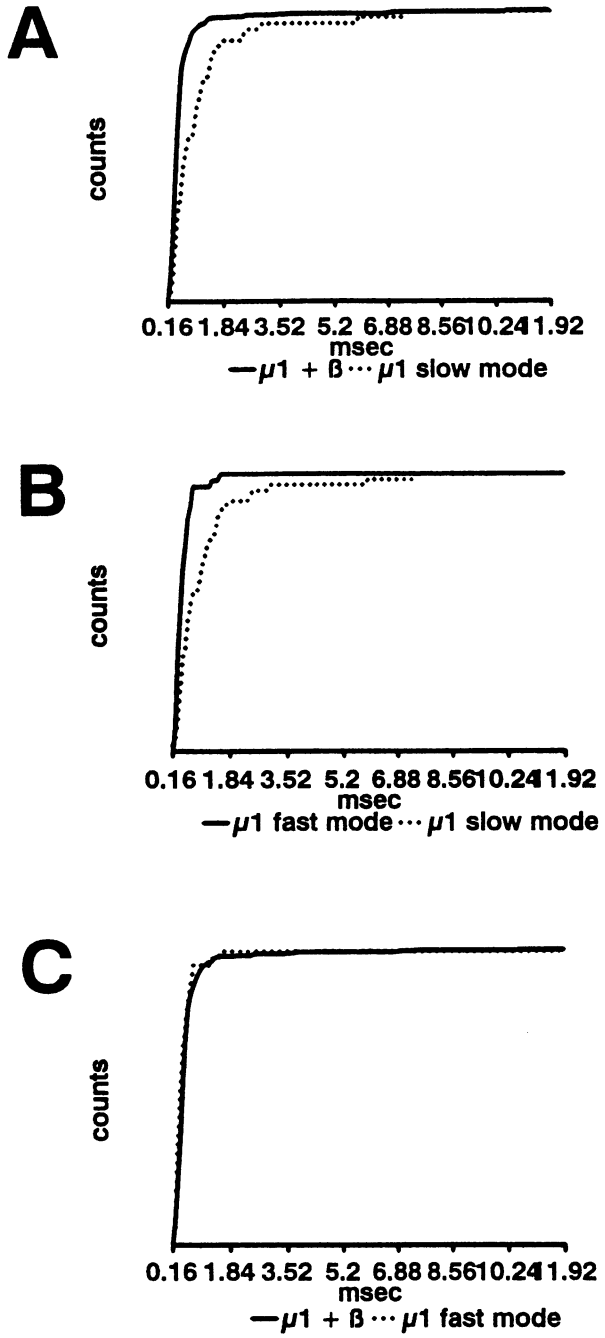


FIGURE 8 Cumulative first latencies for $\mu 1$ and $\mu 1 + \beta_1$ suggest that activations for the fast mode of $\mu 1$ and for $\mu 1 + \beta_1$ are identical (*C*), and suggest that activation for the fast mode of $\mu 1$ (and thus $\mu 1 + \beta_1$) is more rapid than activation for the slow mode of $\mu 1$ alone (*A, B*). The fast mode of $\mu 1$ was identified when $P_o < 0.010$, and the slow mode was identified when $P_o > 0.200$. The times for first latency to reach half-maximum value ($t_{½}$) for $\mu 1 + \beta_1$ and the fast mode of $\mu 1$ were 0.450 ms and 0.400 ms, respectively, at −20 mV. The $t_{½}$ for the slow mode of $\mu 1$ was 0.700 ms at −20 mV. These data were collected in true single-channel patches at 22°C.

Additionally, the data suggest that the activation rates of $\mu 1 + \beta_1$ and of the fast mode of $\mu 1$ alone are not different (Fig. 8).

## DISCUSSION

### $\mu 1$ undergoes mode shifting

Our single-channel studies of $\mu 1$ expressed in *Xenopus* oocytes demonstrate modal gating, with at least two kinetic schemes. Although mode shifting also occurs for mammalian noncardiac $\alpha$-subunits in transfected mammalian cells (Ukomadu et al., 1992; Cannon and Strittmatter, 1993), it occurs to a greater degree in oocytes. Slow-mode behavior is evidenced by prominant bursting, whereas fast mode

behavior is evidenced by one or two discrete openings that occur early in a test pulse. Slow-mode behavior is clustered and remains evident throughout the duration of the patch. The ensemble average for $\mu$1 shows the characteristic $I_{Na}$ with fast and slow decay components associated with the fast and slow modes, respectively. The histogram of number of openings per sweep suggests different kinetic behaviors in which sweeps demonstrate only single openings or bursts of about 20 openings (Fig. 1 *F*).

Because modal opening behavior occurs, multiple open states ought to be detectable. Analysis of a representative open-time histogram for $\mu$1 alone resulted in the detection of two MOTs of ~0.5 ms and ~1.5 ms at −20 mV. Exponential fits of other open-time histograms at various test potentials showed that two open states could be detected at −40, −20, and 0 mV (Fig. 3). Although technically difficult to separate the modes precisely, the fast mode was shown to be associated with the short open time, whereas the slow mode was associated with the long open time.

The slow and the fast modes could be favored in $\mu$1 either with alterations in step frequency or with changes in the holding potential. The slow mode predominated when the interpulse intervals were prolonged (≥20 s) and when the holding potential was hyperpolarized (more negative than −100 mV). The fast mode predominated when interpulse intervals were short (≤300 ms) and the holding potentials were depolarized (~ −60 to −80 mV). There are two possible and perhaps related mechanisms for this rate-dependent effect. First, inactivation of the high $P_o$ slow mode might occur, leaving only those channels in the fast mode to gate. There is a decrease in peak $I_{Na}$ during rapid depolarizations, as expected if the slow mode does not have time to recover completely. Second, channels must exchange between the fast and slow modes. When depolarization frequencies are very slow (e.g., interpulse interval of 20 s), no fast decay can be seen in the oocyte current, so the channels must be predominantly in the slow mode. At high depolarization frequencies (e.g., 3.3 Hz), it appears that the transition from the slow to fast mode must be favored, so that channels can continue to gate. The most obvious reason that transfer from the slow mode to the fast mode must occur is the fact that $I_{Na}$ does not disappear during rapid depolarizations. If inactivation of the slow mode was the only mechanism for favoring the fast mode, $I_{Na}$ would disappear, because all channels would eventually shift from the fast to slow mode and thus become inactive. Peak $I_{Na}$ in the fast mode is lower in part because the mean open time is shorter.

The fast mode is also prevalent at more depolarized potentials. It is difficult to determine whether the slow mode is preferentially inactivated by the depolarized holding potentials or whether channels shift to the fast mode at more depolarized holding potentials. It seems likely that the dominant mechanism involves slow mode inactivation by more depolarized holding potentials, because the number of overlapping channels found when depolarized holding potentials were maintained was consistently less than the number of overlapping channels found when the holding potential was hyperpolarized within the same patch (data not shown).

The voltage dependence and the frequency dependence of these two different modes, in vivo, might be an important factor if the slow mode can exist under physiological conditions. It is possible that the first few action potentials in a train might be prolonged, but during rapid signaling $Na^+$ channels would be unable to gate in the slow mode, and thus action potential duration would be shorter. Furthermore, because recovery from inactivation of the slow mode is probably prolonged, slow mode behavior is limited, thus preventing excessive prolongation of action potentials.

## The role of the $\beta_1$-subunit in restoring rapid current decay

Schreibmayer et al. (1994) suggested that the $\beta_1$-subunit restored rapid decay to $\mu$1 expressed in *Xenopus* oocytes by enhancing inactivation and thus by decreasing MOTs. In their study, the MOT of $\mu$1 decreased from 1.4 ± 0.8 ms to 0.3 ± 0.1 ms at −10 mV upon coexpression of $\beta_1$. These MOTs are surprisingly similar to the MOTs measured in our experiments, except that Schreibmayer et al. apparently only found single MOTs for $\mu$1 and $\mu$1 + $\beta_1$, rather than the mixed populations found in this study.

Examination of our single-channel current traces show that $\mu$1 + $\beta_1$ behaves exactly as the fast mode of $\mu$1 alone. Furthermore, the $NP_o$ history for $\mu$1 + $\beta_1$ shows that low $P_o$ sweeps predominate. Perhaps most convincingly, analysis of an open-time histogram for $\mu$1 + $\beta_1$ at −20 mV results in detection of the same MOTs as seen for $\mu$1 alone. Analysis of open-time histograms confirms that the open states for $\mu$1 and $\mu$1 + $\beta_1$ are identical (Fig. 2). Coexpression of $\beta_1$ reduced the size of the long MOT component without altering the two open states. Finally, ensemble averages of both single-channel patches and macropatches shows that currents of $\mu$1 + $\beta_1$ are identical to currents of the fast mode of $\mu$1 alone. It seems likely that $\beta_1$ favors a protein conformation in which fast gating predominates.

## $\beta_1$-subunit affects the activation pathway

In studies using the two-electrode voltage clamp, time to peak $I_{Na}$ appears faster when $\beta_1$ is present than when it is not present (Isom et al., 1992; Patton et al., 1994), and this has led to the impression that the $\beta_1$-subunit speeds activation. However, macroscopic $I_{Na}$ cannot be used unequivocally to demonstrate an increase in the rate of activation because time to peak $I_{Na}$ is influenced by MOT, as clearly demonstrated by the simulation. An additional problem is introduced in scaling currents under different conditions to the same peak value for comparison, because distortion of the time course of activation can occur. Similarly, distortion of the time courses via normalization would cause the first latency for the slow mode to appear faster than actually occurs when the slow mode component is smaller than the

fast mode, as in our experiments. As seen in Fig. 8, even with the distortion, activation of the fast mode is faster relative to activation of the slow mode. Furthermore, the actual measurements of $t_{1/2}$ indicate that fast mode activation is more rapid. These results and those of Zhou et al. (1991) make it apparent that the $\beta_1$-subunit enhances the rate of activation.

## Possible kinetic models

Identification of $\beta_1$-subunit effects on the activation pathway is important in deciding on a kinetic model. If activation pathways for the fast mode ($\mu 1 + \beta_1$) and the slow mode of $\mu 1$ are identical, then the only rate constant that needs to vary is that entering the inactivated state from the open state. This would result in the following Markovian model:

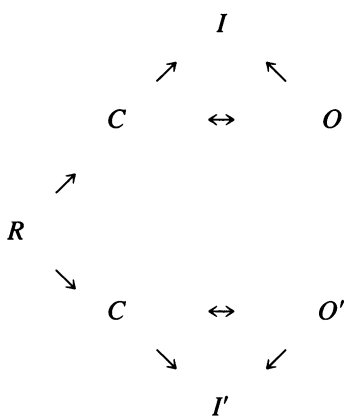


where $R$ represents all closed states left of the final closed state in each of the pathways. This is the simplest model possible based on the evidence presented in this paper. Differences in the $O \rightarrow I$ transition can wholly account for the different mean open times. On the other hand, if the activation pathways between the fast mode and the slow mode of $\mu 1$ are different, then the following model must be considered:

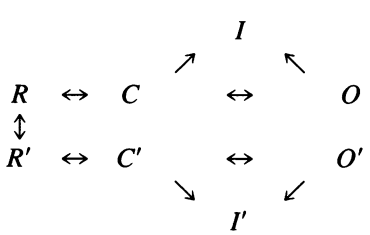


in which the mode shift might occur in any of the closed states, where the probability of shifting from one mode to the other is itself dependent on holding potential, frequency of depolarizations, and the presence of the $\beta_1$-subunit. Conditions favoring native-like fast gating include a depolarized holding/resting potential, rapid signaling, and the presence of the $\beta_1$-subunit. Conversely, conditions favoring slow gating include a hyperpolarized holding/resting potential, slow signaling, and the absence of the $\beta_1$-subunit.

The authors appreciate the generous advice and support of Dr. Aaron Fox and Dr. John Kyle.

The work was supported by National Institutes of Health grants PO1-HL20592 (HAF) and T32-HD07009 (SYC).

## REFERENCES

Alzheimer, C., P. C. Schwindt, and W. E. Crill. 1993. Modal gating of $Na^+$ channels as a mechanism of persistent $Na^+$ current in pyramidal neurons from rat and cat sensorimotor cortex. *J. Neurosci.* 13:660–673.

Bezanilla, F., and C. M. Armstrong. 1977. Inactivation of the sodium channel. I. Sodium current experiments. *J. Gen. Physiol.* 70:549–566.

Böhle, T., and K. Benndorf. 1995. Multimodal action of single $Na^+$ channels in myocardial mouse cells. *Biophys. J.* 68:121–130.

Cannon, S. C., A. I. McClatchey, and J. F. Gusella. 1993. Modification of the $Na^+$ current conducted by the rat skeletal muscle $\alpha$ subunit by coexpression with a human brain $\beta$ subunit. *Pflugers Arch.* 423: 155–157.

Cannon, S. C., and S. M. Strittmatter. 1993. Functional expression of sodium channel mutations identified in families with periodic paralysis. *Neuron.* 10:317–326.

Colquhoun, D., and F. Sigworth. 1983. Fitting and statistical analysis of single-channel records. *In* Single-Channel Recording. B. Sakmann and E. Neher, editors. Plenum Press, New York. 191–263.

Delcour, A. H., D. Lipscombe, and R. W. Tsien. 1993. Multiple modes of N-type calcium channel activity distinguished by differences in gating kinetics. *J. Neurosci.* 13:181–194.

Delcour, A. H., and R. W. Tsien. 1993. Altered prevalence of gating modes in neurotransmitter inhibition of N-type calcium channels. *Science.* 259:980–984.

Fleig, A., P. Ruben, and M. Rayner. 1994. Kinetic mode switch of rat brain IIa Na channels in *Xenopus* oocytes excised macropatches. *Pflugers Arch.* 427:399–405.

Goldin, A. L., T. Snutch, H. Lubbert, A. Dowsett, J. Marshall, V. Auld, W. Downey, L. C. Fritz, H. A. Lester, R. Dunn, W. A. Catterall, and N. Davidson. 1986. Messenger RNA coding for only the $\alpha$ subunit of the rat brain Na channel is sufficient for expression of functional channels in *Xenopus* oocytes. *Proc. Natl. Acad. Sci. USA.* 83:7503–7507.

Hebert, T. E., P. Drapeau, and R. J. Dunn. 1994. Characterization of fast and slow gating modes of the RIIA voltage-gated sodium channel expressed in oocytes with an improved two-electrode voltage clamp. *Biophys. J.* 66:A102.

Hess, P., J. B. Lansman, and R. W. Tsien. 1984. Different modes of Ca channel gating behavior favoured by dihydropyridine Ca agonists and antagonists. *Nature.* 311:538–544.

Isom, L. L., K. S. De Jongh, D. E. Patton, B. F. X. Reber, J. Offord, H. Charbonneau, K. Walsh, A. L. Goldin, and W. A. Catterall. 1992. Primary structure and functional expression of the $\beta_1$ subunit of the rat brain sodium channel. *Science.* 256:839–842.

Ji, S., W. Sun, A. George, R. Horn, and R. Barchi. 1994. Voltage-dependent regulation of modal gating in the rat SkM1 sodium channel expressed in *Xenopus* oocytes. *J. Gen. Physiol.* 104:625–643.

Krieg, P. A., and D. A. Melton. 1984. Functional messenger RNAs are produced by SP6 in vitro transcription of cloned cDNAs. *Nucleic Acids Res.* 12:7057–7070.

McManus, O. B., and K. L. Magelby. 1988. Kinetic states and modes of single large-conductance calcium-activated potassium channels in cultured rat skeletal muscle. *J. Physiol. (Lond.).* 402:79–120.

Methfessel, C., V. Witzemann, T. Takahasi, M. Mishina, S. Numa, and B. Sakmann. 1986. Patch clamp measurements on *Xenopus laevis* oocytes: currents through endogenous channels and implanted acetylcholine receptor and sodium channels. *Pflugers Arch.* 407:577–588.

Moczydlowski, E., and R. Latorre. 1983. Gating kinetics of $Ca^{2+}$-activated $K^+$ channels from rat muscle incorporated into planar lipid bilayers:

evidence for two voltage-dependent $Ca^{2+}$ binding reactions. *J. Gen. Physiol.* 82:511–542.

Moorman, J. R., G. E. Kirsch, A. M. J. VanDongen, R. H. Joho, and A. M. Brown. 1990. Fast and slow gating of sodium channels encoded by a single mRNA. *Neuron.* 4:243–252.

Naranjo, D., and P. Brehm. 1993. Modal shifts in acetylcholine receptor channel gating confer subunit-dependent desensitization. *Science.* 260: 1811–1814.

Nilius, B. 1988. Modal gating behavior of cardiac sodium channels in cell-free membrane patches. *Biophys. J.* 53:857–862.

Patlak, J. B. 1988. Sodium channel subconductance levels measured with a new variance-mean analysis. *J. Gen. Physiol.* 92:413–430.

Patlak, J. B., K. A. F. Gration, and P. N. R. Usherwood. 1979. Single glutamate-activated channels in locust muscle. *Nature (Lond.).* 278: 643–645.

Patlak, J. B., and M. Ortiz. 1985. Slow currents through single sodium channels of the adult rat heart. *J. Gen. Physiol.* 86:89–104.

Patlak, J. B., and M. Ortiz. 1986. Two modes of gating during late $Na^+$ channel currents in frog sartorius muscle. *J. Gen. Physiol.* 87:305–326.

Patton, D., L. Isom, W. Catterall, and A. Goldin. 1994. The adult rat brain $\beta_1$ subunit modifies activation and inactivation gating of multiple sodium channel $\alpha$ subunits. *J. Biol. Chem.* 269:17649–17655.

Plummer, M. R., and P. Hess. 1991. Reversible uncoupling of inactivation in N-type calcium channels. *Nature.* 351:657–659.

Provencher, S. W. 1976. A Fourier method for the analysis of exponential decay curves. *Biophys. J.* 16:27–41.

Satin, J., J. W. Kyle, M. Chen, R. B. Rogart, and H. A. Fozzard. 1992. The cloned cardiac Na channel $\alpha$-subunit expressed in *Xenopus* oocytes show gating and blocking properties of native channels. *J. Membr. Biol.* 130:11–22.

Scanley, B. E., D. A. Hanck, T. Chay, and H. A. Fozzard. 1990. Kinetic analysis of single sodium channels from canine cardiac Purkinje cells. *J. Gen. Physiol.* 95:411–437.

Schreibmayer, W., M. Wallner, and I. Lotan. 1994. Mechanism of modulation of single sodium channels from skeletal muscle by the $\beta_1$-subunit from rat brain. *Pflugers Arch.* 426:360–362.

Sigworth, F., and E. Neher. 1980. Single $Na^+$ channel currents observed in cultured rat muscle cells. *Nature (Lond.).* 287:447–449.

Trimmer, J. S., S. S. Cooperman, S. A. Tomiko, J. Zhou, S. M. Crean, M. B. Boyle, R. G. Kallen, Z. Sheng, R. L. Barchi, F. J. Sigworth, R. H. Goodman, W. S. Agnew, and G. Mandel. 1989. Primary structure and functional expression of a mammalian skeletal muscle sodium channel. *Neuron.* 3:33–49.

Ukomadu, C., J. Zhou, F. J. Sigworth, and W. S. Agnew. 1992. $\mu$1 $Na^+$ channels expressed transiently in human embryonic kidney cells: biochemical and biophysical properties. *Neuron.* 8:663–676.

Wallner, M., L. Weigl, P. Meera, and I. Lotan. 1993. Modulation of the skeletal muscle sodium channel $\alpha$-subunit by the $\beta_1$-subunit. *FEBS Lett.* 336:535–539.

Weiss, R., and R. Horn. 1986. Functional differences between two classes of sodium channels in developing rat skeletal muscle. *Science.* 233: 361–364.

Yang, J. S., P. B. Bennett, N. Makita, A. L. George, and R. L. Barchi. 1993. Expression of the sodium channel $\beta_1$ subunit in rat skeletal muscle is selectively associated with the tetrodotoxin-sensitive $\alpha$ subunit isoform. *Neuron.* 11:915–922.

Zhou, J., J. F. Potts, J. S. Trimmer, W. S. Agnew, and F. J. Sigworth. 1991. Multiple gating modes and the effect of modulating factors on the $\mu$I sodium channel. *Neuron.* 7:775–785.